Disclosing the Properties of a New Ce(III)-Based MOF: Ce2(NDC)3(DMF)2

Supporting information for:

Disclosing the properties of a new Ce(III)-based MOF: $Ce_2(NDC)_3(DMF)_2$

Cesare Atzori[a], Kirill A. Lomachenko[b], Sigurd Øien-Ødegaard[c], Carlo Lamberti[d,e], Norbert Stock[f], Claudia Barolo[a], Francesca Bonino[a *]

[a] Department of Chemistry, NIS and INSTM Reference Centre, Università di Torino, Via G. Quarello 15, I-10135 and Via P. Giuria 7, I-10125 Torino, Italy
[b] European Synchrotron Radiation Facility, 71 Avenue des Martyrs, CS 40220, 38043 Grenoble Cedex 9, France
[c] Department of Chemistry, University of Oslo, P.O. Box 1033, N-0315 Oslo, Norway
[d] Department of Physics, INSTM Reference Center and CrisDi Interdepartmental Centre for Crystallography, Università di Torino, Via P. Giuria 1, I-10125 Torino, Italy
[e] The Smart Materials Research Institute, Southern Federal University, A. Sladkova str. 178/24, 344090 Rostov-on-Don, Russia
[f] Institut für Anorganische Chemie, Christian-Albrechts-Universität zu Kiel, Max-Eyth-Straße 2, 24118 Kiel, Germany

[*]Corresponding author e-mail: francesca.bonino@unito.it

Outline:

1. Review of the Ce(III) based MOFs

Table S1 – MOFs with Ce(III) cations, a selection of what is reported in ref.[1]

Formula	Linker molecule	Reference
$[Ce_2(L)_2(DMF)_4]$	4,4',4''-{[(2,4,6-trimethylbenzene-1,3,5-triyl)tris-(methylene)] tris(oxy)}tribenzoic acid	2
$[Ce(HTCPB)]\cdot(EtOH)_{0.28}\cdot(H_2O)_{2.75}$	1,2,4,5-Tetrakis(4-carboxyphenyl)benzene	3
$[Ce(BTC)(DMF)_2]$	Trimesic acid	4
$[Ce_5(BDC)_{7.5}(DMF)_4]$	Terephthalic acid	5
$[Ce_2(ADC)_3(DMF)_4]\cdot DMF$	9,10-Anthracenedicarboxylic acid	6
$[Ce(ADC)_{1.5}(DMA)_3]$	9,10-Anthracenedicarboxylic acid	6
$[Ce(BTC)(H_2O)]\cdot DMF$	Trimesic acid	7,8
$[Ce_2(H_2O)(BPyDC)_3(DMF)_2]\cdot 2(DMF)$	2,2-Bipyridine-5,5'-dicarboxylic acid	9
$[Ce_4(H_2O)_5(BPyDC)_6(DMF)]\cdot x(DMF)$	2,2-Bipyridine-5,5'-dicarboxylic acid	9
$[Ce(TTTPC)(NO_2)_2Cl]\cdot H_2O_{10}$	1,1',1''-tris(2,4,6-trimethylbenzene-1,3,5- triyl)-tris(methylene)-tris(pyridine-4-carboxylic acid)}	10
$[Ce_2(EBTC)_{1.5}(CH_3OH)_4]\cdot 6H_2O$	1,1'-ethynebenzene-3,3′,5,5′-tetracarboxylic acid	11
$[Ce(HL)(DMA)_2]\cdot DMA\cdot 2H_2O$	5,5'-(2,3,5,6-tetramethyl-1,4-phenylene) bis(methylene) bis(azanediyl) diisophthalic acid	12
$[Ce_2(BPDA)_3(H_2O)_4]\cdot H_2O$	Benzophenone-2,4'-dicarboxylic acid	13
$[Ce_2(NDC)_3(DMF)_4]\cdot xH_2O$	1,4-Naphthalenedicarboxylic acid	14
$[Ce(NDC)_{1.5}(DMF)(H_2O)_{0.5}]\cdot 0.5DMF$	2,6-Naphthalenedicarboxylic acid	15
$[Ce(PDC)_{1.5}(DMF)]\cdot DMF$	3,5-Pyridinedicarboxylic acid	16,17
$[Ce_2(PDC)_3(H2O)_2]$	3,5-Pyridinedicarboxylic acid	18
[CeCl(BPDC)(DMF)]	4,4'-Biphenyldicarboxylic acid	19
$[Ce(BTPCA)(H_2O)]\cdot 2DMF\cdot 3H_2O$	1,1',1''-(benzene-1,3,5-triyl)tripiperidine-4-carboxylic acid	20
$[Ce_2(DHBDC)_3(DMF)_4]\cdot DMF$	Benzene-2,5-dihydroxy-1,4-dicarboxylic acid	21
$[Ce_6(BDC)_9(DMF)_6(H_2O)_3]\cdot 33DMF$	Terephthalic acid	22
$[Ce_2(ADB)_3(DMSO)_4]\cdot 6DMSO\cdot 8H_2O$	4,4'-Azodibenzoic acid	22
$[Ce_3(ADB)_3(HADB)_3]\cdot 33DMSO\cdot 29H_2O$	4,4'-Azodibenzoic acid	22

$[Ce_2(ADB)_3(H2O)_3]$	4,4'-Azodibenzoic acid	22
$[Ce_2(SDBA)_3(DMF)_4]$	4,4'-Sulfonyldibenzoic acid	23
$[(CH_3)_2NH_2]_3[Ce_3(SDBA)_6]\cdot 6DMF$	4,4'-Sulfonyldibenzoic acid	23
$[Ce(BTB)(H_2O)]$	1,3,5-Tris(4-carboxyphenyl)benzene	24
$[Ce_2(PDA)_3(H_2O)]\cdot 2H_2O$	1,4 Phenylendiacetic acid	25

2. $Ce_2(NDC)_3$ X-ray single-crystal diffraction

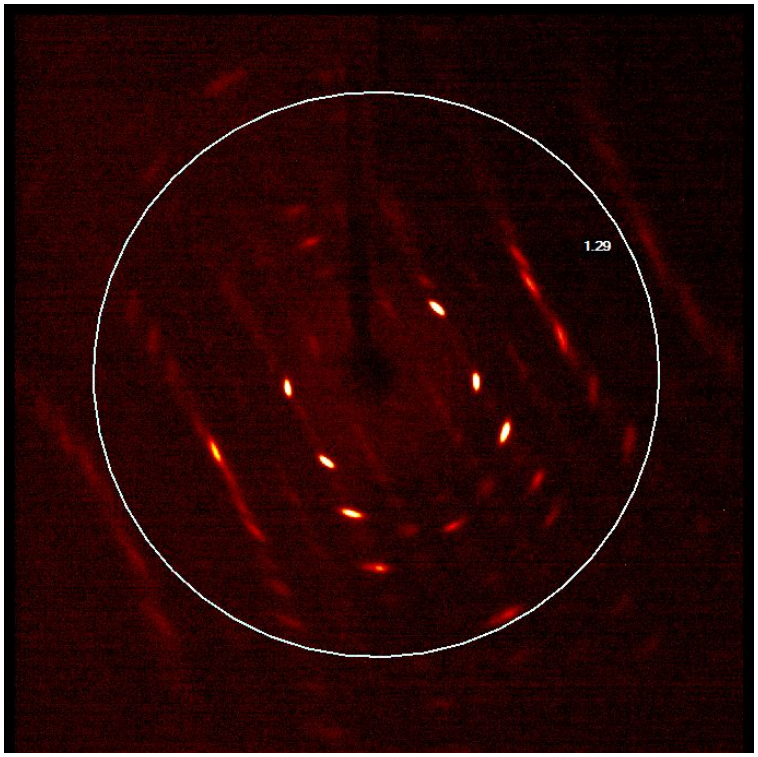

Figure S1 – Representative diffraction frame from $Ce_2(NDC)_3$, with frame width 0.5°. The circle shows the data cut-off at 1.29 Å, as the diffraction at higher angles could not be integrated.

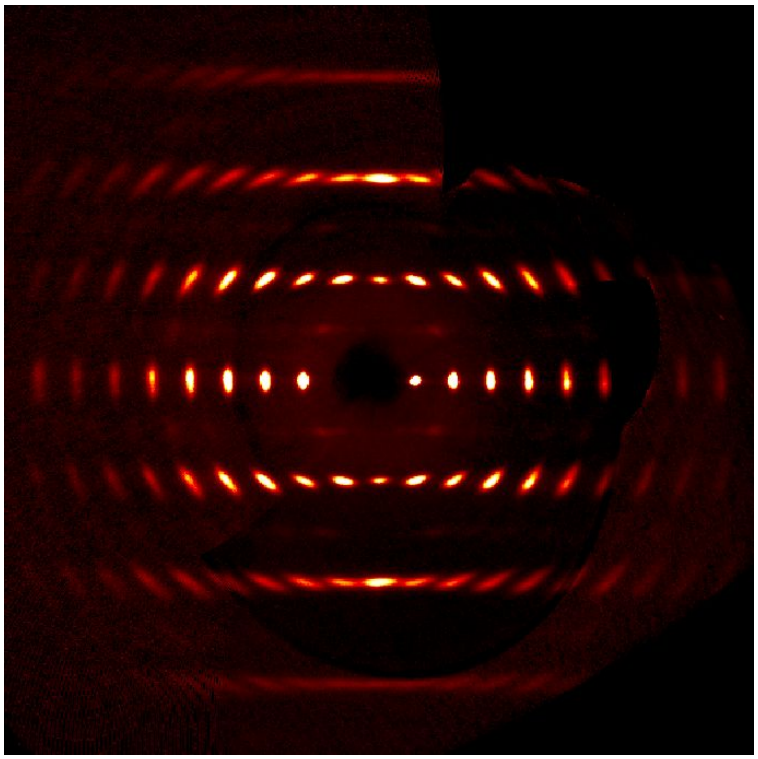

Figure S2 – Precession image of the diffraction from $Ce_2(NDC)_3$ showing the 0kl plane.

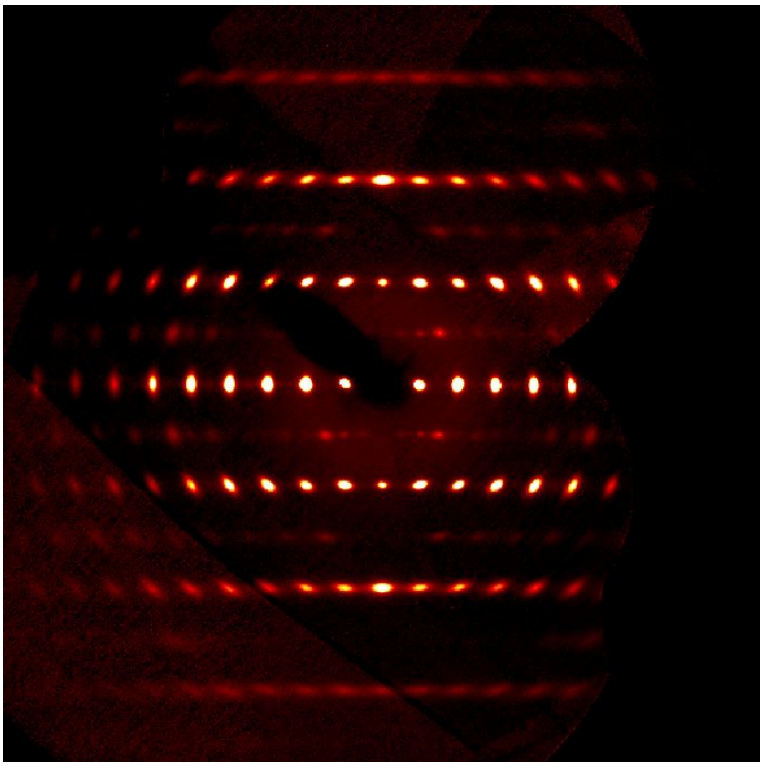

Figure S3 – Precession image of the diffraction from $Ce_2(NDC)_3$ showing the h0l plane.

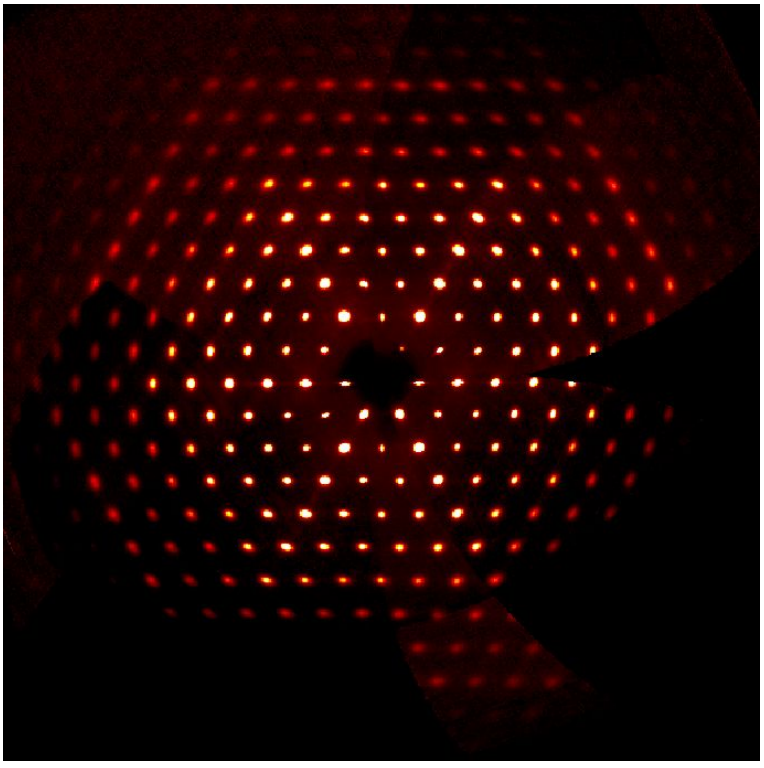

Figure S4 – Precession image of the diffraction from $Ce_2(NDC)_3$ showing the hk0 plane.

3. $Ce_2(NDC)_3$ structure details

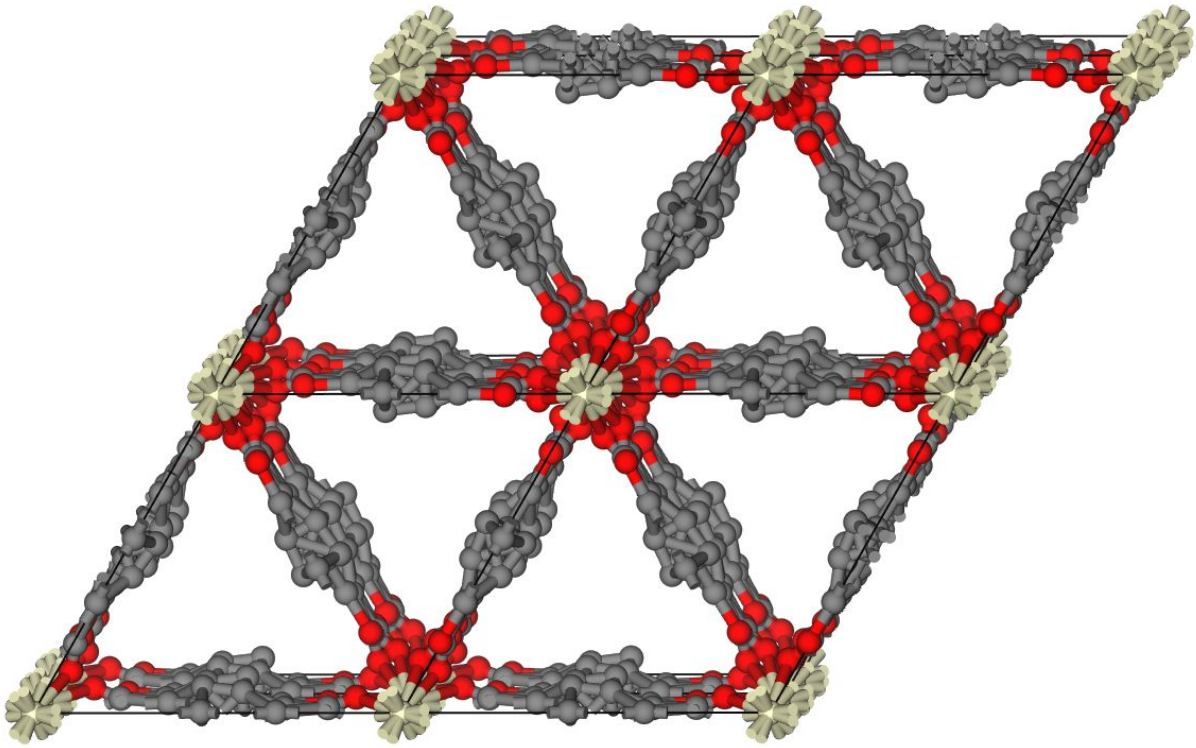

Figure S5 –Crystal structure of $Ce_2(NDC)_3$ viewed along the c-axis, showing all possible positions of the atoms.

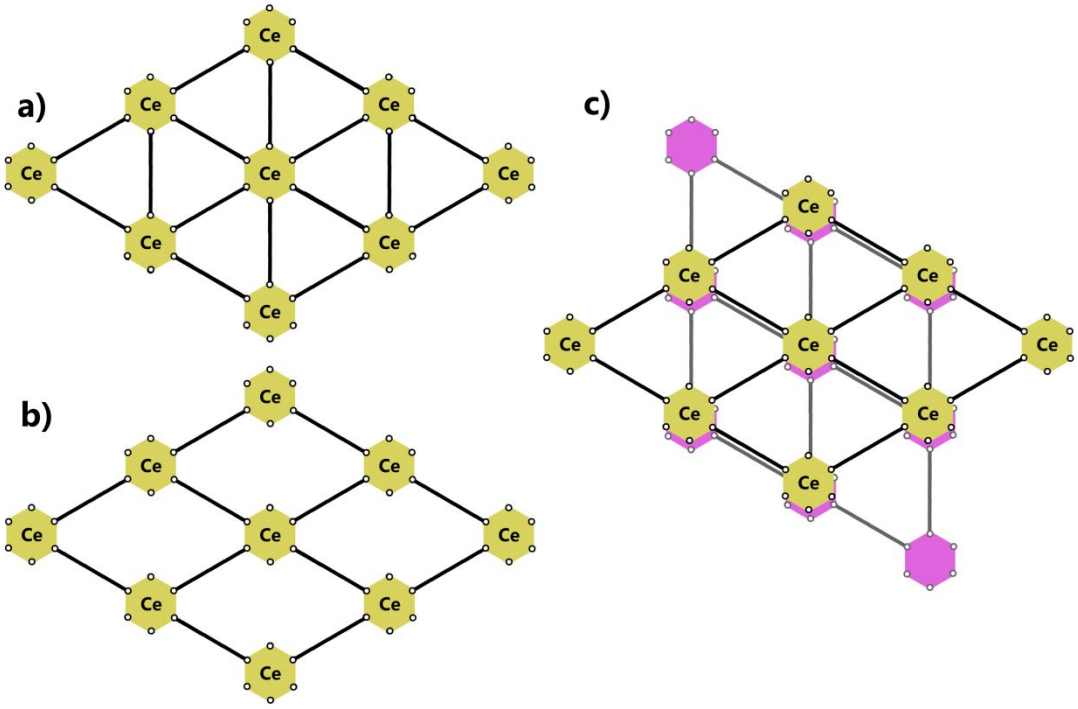

Figure S6 – Schematic representations of the structure of the activated MOF, viewed along the c-axis. a) Hexagonal unit cell. b) Orthorhombic cell. c) Two overlapping twin domains of the orthorhombic structure, showing the apparent hexagonal symmetry.

4. Powder diffraction pattern of $Ce_2(NDC)_3$ contacted with DMF after activation

In order to shed light on the reversibility of the solvation-desolvation process of pristine $Ce_2(NDC)_3(DMF)_2$, $Ce_2(NDC)_3$ was put again in contact with DMF by immersion for 15 minutes at room temperature. The powder diffraction pattern of the material after such a treatment, shown in Figure S7, demonstrates the irreversibility of the process in the adopted conditions.

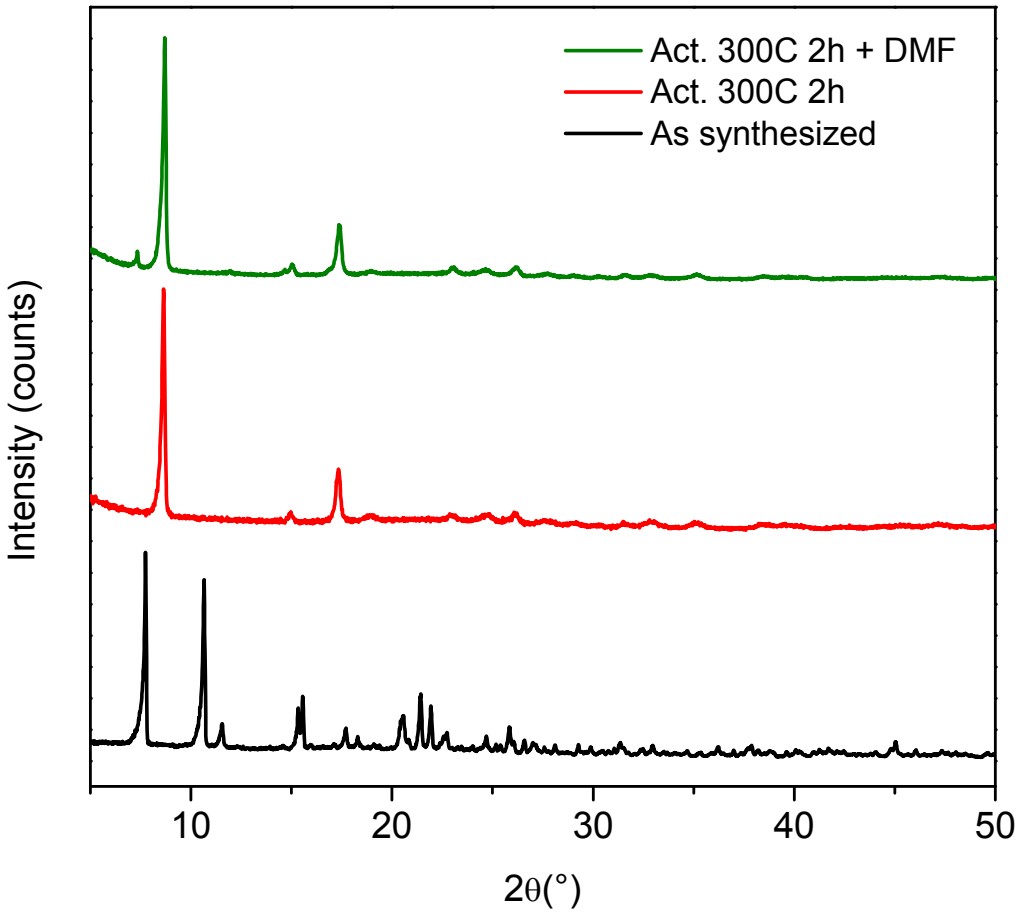

Figure S7 – Powder diffraction data of pristine $Ce_2(NDC)_3(DMF)_2$ (black curve), $Ce_2(NDC)_3$ (red curve) and $Ce_2(NDC)_3$ upon DMF contact (dark green curve).

5. In-situ FTIR spectra of CO adsorbed on $Ce_2(NDC)_3$ at low temperature

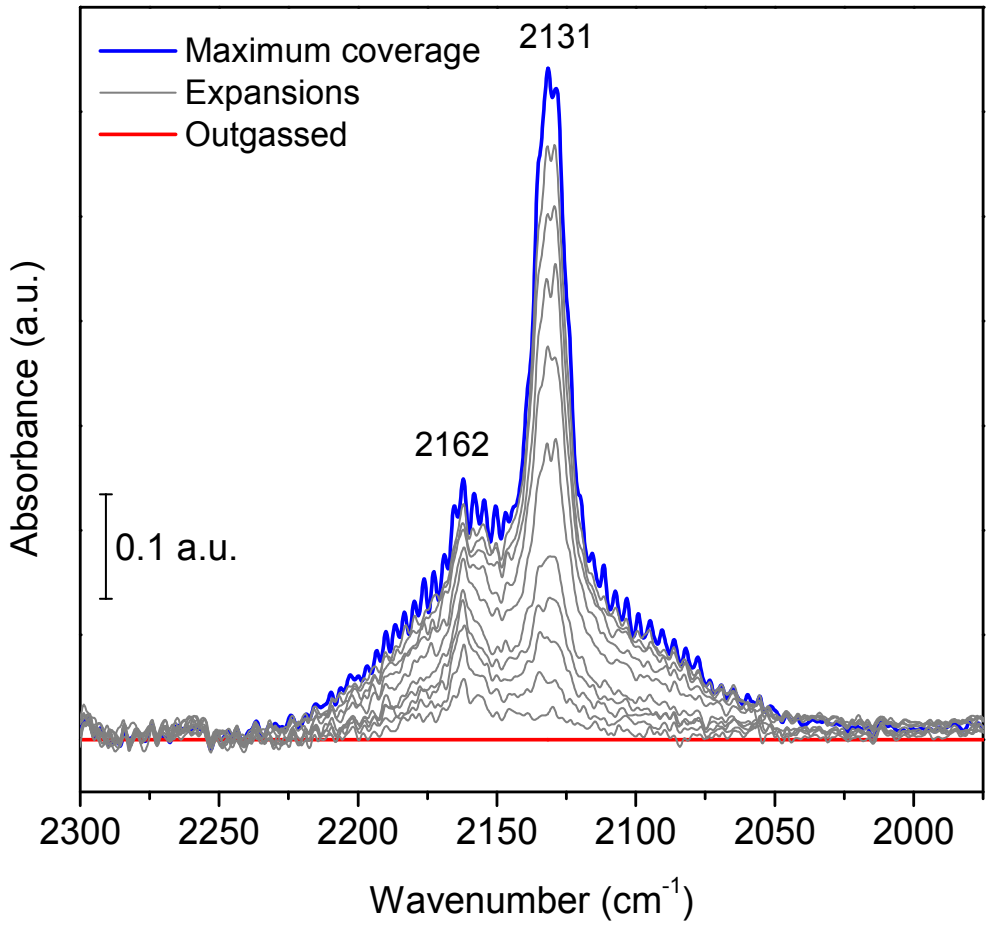

Figure S8 – Background subtracted FTIR spectra of CO adsorption at about 100K for $Ce_2(NDC)_3$. Maximum and intermediate coverages are represented by the blue curve and the grey curves, respectively.

CO was dosed as a probe molecule during an in-situ FTIR spectroscopy[26] experiment performed on a self-supporting pellet of $Ce_2(NDC)_3$. The temperature was then decreased to about 100K using a home made cell cooled down with liquid nitrogen. Figure S8 reports the spectra taken during the desorption procedure.

Under the typical roto-vibrational spectrum of gaseous CO[27] which is clearly visible in the blue curve, two main signals of adsorbed CO are evident at 2162 and 2131 cm^{-1}, respectively. The latter (which is the first to be removed upon outgassing) is readily ascribable to physisorbed CO condensed in the pores while the other one can be assigned to CO interacting with acidic Ce^{3+} sites[8,28].

6. EXAFS fitting details

According to the XRD data, the sets of Ce-L distances (L being a light atom: O or C) of the nearest shells exhibit certain preferred values. Therefore, in order to decrease the amount of parameters for the EXAFS fitting and make the fit more robust, each of the four subsets of the scattering paths (Ce-O or Ce-C in both solvated and activated compounds) can be reasonably approximated by three groups with different Ce-L distance (Figure S9). The corresponding interatomic distances indicated in Figure S9 were used as initial values for three separate Ce-O and Ce-C shells during EXAFS fitting. Coordination numbers were set according to the XRD occupancies and kept fixed in the fitting procedures. Each of the three oxygen shells in the solvated material was parametrized with the same expansion/contraction parameter, scaled linearly with the corresponding Ce-O distance. Such approach was used also for the Ce-C and Ce-O shells in the hydrated and activated materials respectively. Conversely, each of the three Ce-C shells in the activated material were parametrized with a separate ΔR parameter. Four separate Debye-Waller (DW) parameters were used to parametrize the four above mentioned groups of shells, scaling within each group being as a square root of R. Finally, a separate ΔR and DW factor were assigned to Ce-Ce shell in the activated material. The amplitude reduction factor was fixed to $S_0^2 = 1$, which has proven to be a reasonable approximation for Ce K-edge EXAFS in porous material.[29]

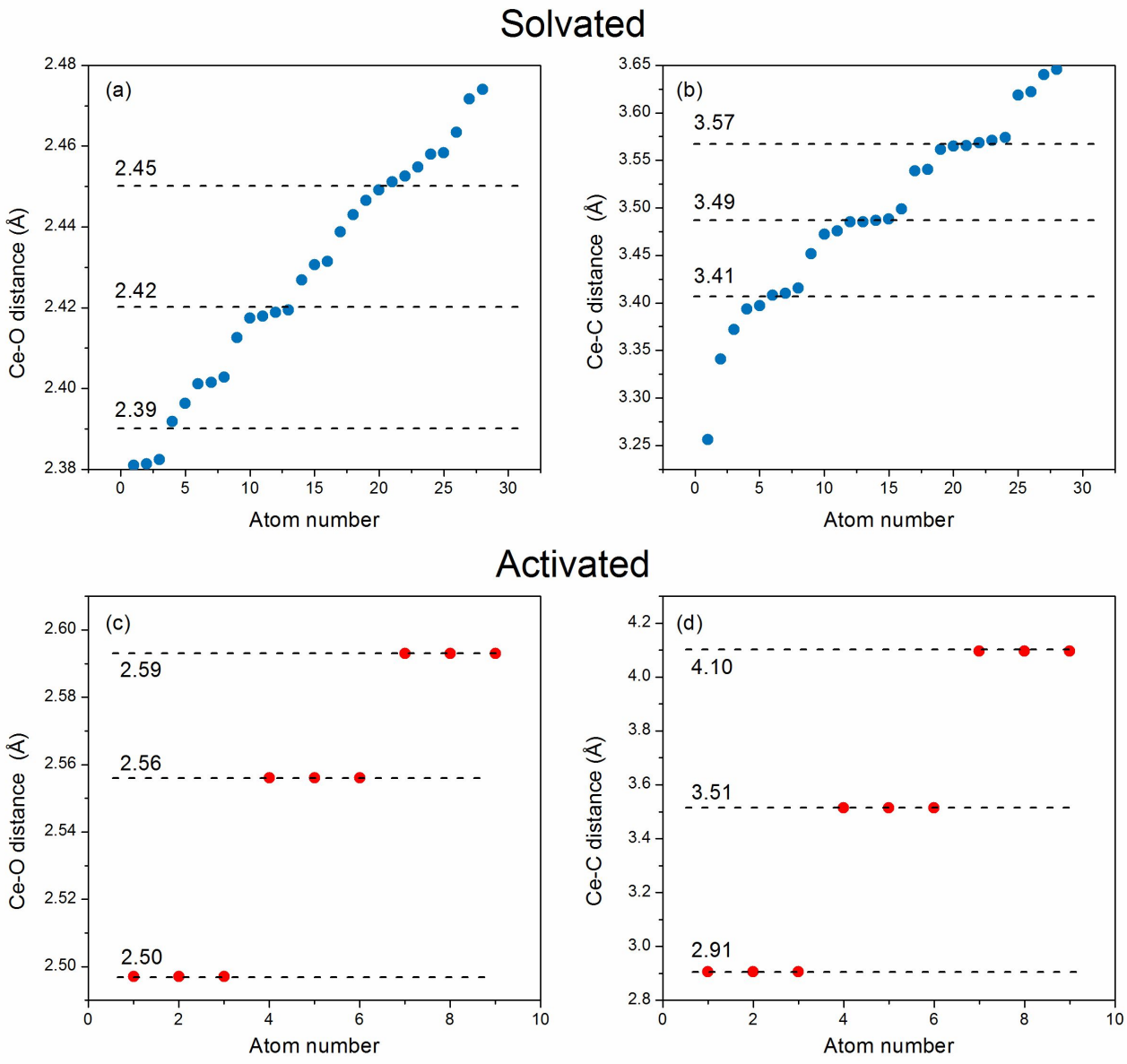

Figure S9 - Distances between Ce and the nearest O (left) and C (right) atoms in the solvated (top) and activated (bottom) materials obtained by XRD. Four and one non-equivalent Ce were considered for solvated and activated materials, respectively. Distances employed as initial values for EXAFS fitting are in the Figure by the dashed lines with the corresponding labels.

7. N_2 and CO_2 adsorption isotherms at low temperatures

In order to measure the surface area and the porosity of $Ce_2(NDC)_3$, N_2 was dosed at -196°C. The results (see Figure S10) show a nearly negligible adsorption in the whole pressure range (0-1 p/p_0 range) indicating nil surface area or porosity whatever the model used to reduce this data (e.g. Langmuir or BET models). CO_2 was dosed at a temperature of -78°C as an alternative probe to N_2 in order to address the purpose of measuring a specific surface area on $Ce_2(NDC)_3$ giving a Type I isotherm (see Figure S10).

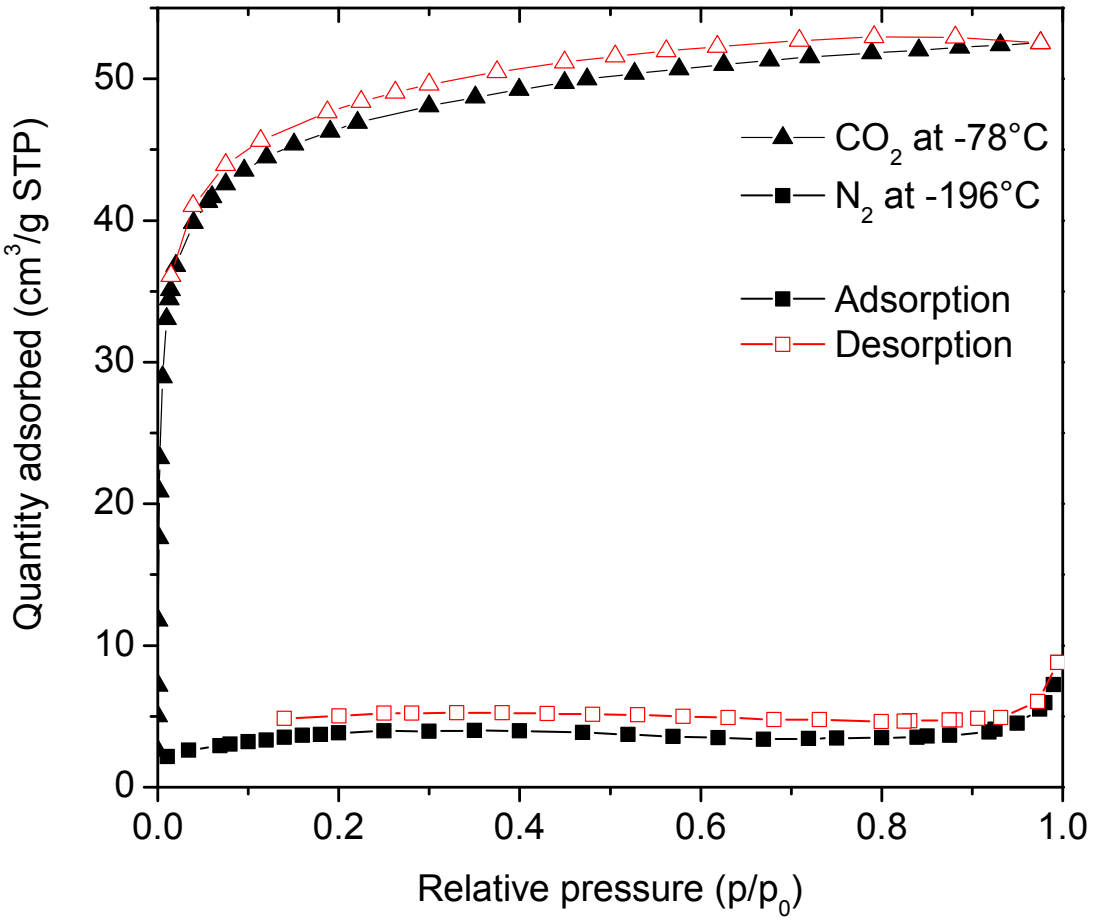

Figure S10 – $Ce_2(NDC)_3$ adsorption isotherms of N_2 at -196°C and CO_2 at -78°C. The two molecules are represented by squares and triangles, respectively. Solid black and open red symbols report the adsorption and desorption branches.

8. IAST Selectivity

The Ideal Adsorbed Solution Theory (IAST)[30] is a method to evaluate and predict the selectivity of competitor gases in a multi-component adsorption process starting from single-component adsorption isotherms. The pyIAST code[31] was used to calculate a CO_2/N_2 IAST selectivity for $Ce_2(NDC)_3$ at 0°C (see Figure S11).

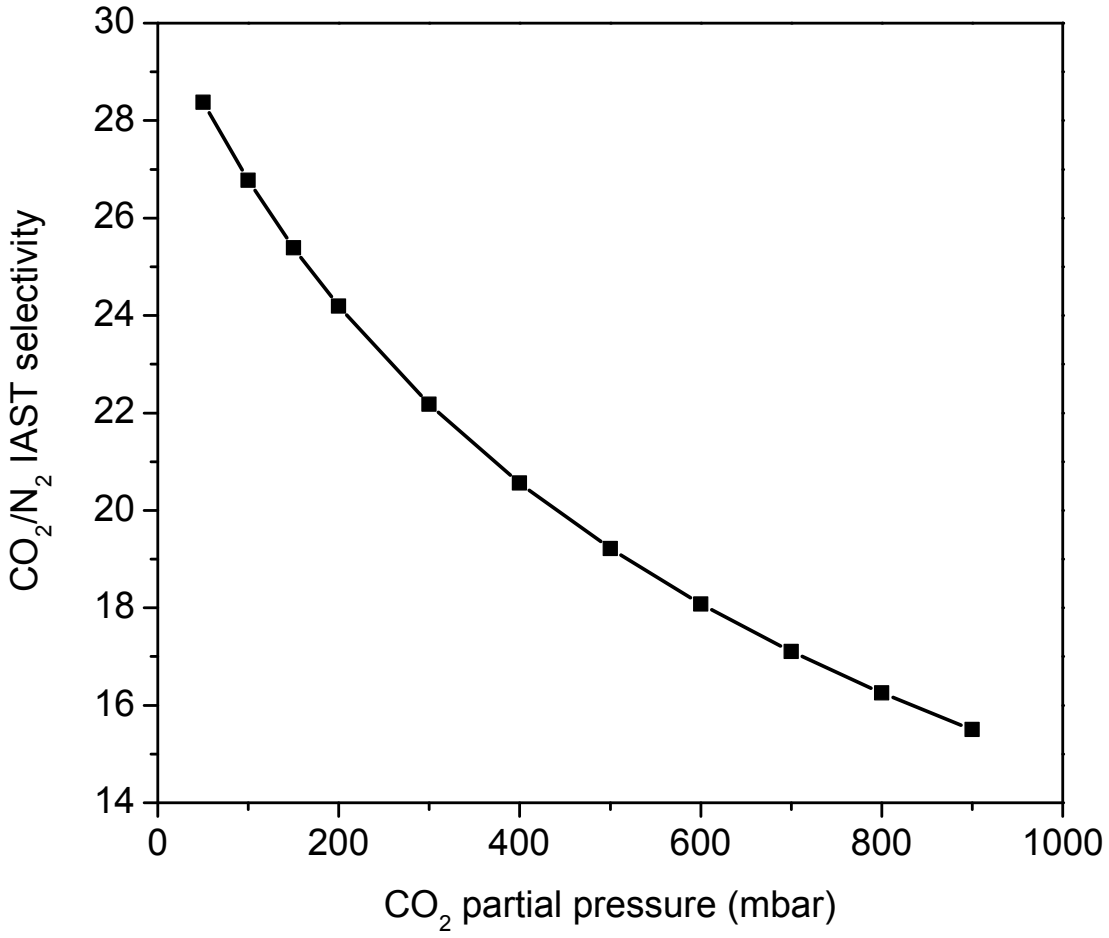

Figure S11 – IAST CO_2/N_2 selectivity factors for a CO_2 / N_2 binary gas mixture at 1 bar of total pressure and a temperature of 0°C.

References

(1) Lammert, M. PhD Thesis, Christian-Albrechts-University, Kiel, 2017.

(2) Liang, L. L.; Xu, L.; Xue, H. B.; Tao, Z. L.; Chen, F. J. Two Metal-Organic Frameworks with Different Configurations Constructed from a Flexible Tripodal Triaromatic Acid. *J. Mol. Struct.* **2016**, *1125*, 656–661.

(3) Warren, J. E.; Perkins, C. G.; Jelfs, K. E.; Boldrin, P.; Chater, P. A.; Miller, G. J.; Manning, T. D.; Briggs, M. E.; Stylianou, K. C.; Claridge, J. B.; et al. Shape Selectivity by Guest-Driven Restructuring of a Porous Material. *Angew. Chemie - Int. Ed.* **2014**, *53*, 4592–4596.

(4) Li, Z.; Liu, K. Poly[(μ(4)-Benzene-1,3,5-Tricarboxyl-Ato)Bis-(N,N-Dimethyl-Formamide)-Cerium(III)]. *Acta Crystallogr. Sect. E. Struct. Rep. Online* **2011**, *67*, m1020.

(5) D'Arras, L.; Sassoye, C.; Rozes, L.; Sanchez, C.; Marrot, J.; Marre, S.; Aymonier, C. Fast and Continuous Processing of a New Sub-Micronic Lanthanide-Based Metal–organic Framework. *New J. Chem.* **2014**, *38*, 1477.

(6) Quah, H. S.; Ng, L. T.; Donnadieu, B.; Tan, G. K.; Vittal, J. J. Molecular Scissoring: Facile 3D to 2D Conversion of Lanthanide Metal Organic Frameworks Via Solvent Exfoliation. *Inorg. Chem.* **2016**, *55*, 10851–10854.

(7) Almáši, M.; Zeleňák, V.; Opanasenko, M.; Císařová, I. Ce(III) and Lu(III) Metal-Organic Frameworks with Lewis Acid Metal Sites: Preparation, Sorption Properties and Catalytic Activity in Knoevenagel Condensation. *Catal. Today* **2015**, *243*, 3098–3114.

(8) Ethiraj, J.; Bonino, F.; Vitillo, J. G.; Lomachenko, K. A.; Lamberti, C.; Reinsch, H.; Lillerud, K. P.; Bordiga, S. Solvent-Driven Gate Opening in MOF-76-Ce: Effect on CO2Adsorption. *ChemSusChem* **2016**, *9*, 713–719.

(9) Ayhan, O.; Malaestean, I. L.; Ellern, A.; Van Leusen, J.; Baca, S. G.; Kögerler, P. Assembly of Cerium(III) 2,2′-Bipyridine-5,5′-Dicarboxylate- Based Metal-Organic Frameworks by Solvent Tuning. *Cryst. Growth Des.* **2014**, *14*, 3541–3548.

(10) Bag, P. P.; Wang, X. S.; Cao, R. Microwave-Assisted Large Scale Synthesis of Lanthanide Metal-Organic Frameworks (Ln-MOFs), Having a Preferred Conformation and Photoluminescence Properties. *Dalton Trans.* **2015**, *44*, 11954–11962.

(11) Zhai, L.; Zhang, W. W.; Ren, X. M.; Zuo, J. L. Luminescent Lanthanide MOFs Based on Conjugated 1,1′-Ethynebenzene-3,3′,5,5′-Tetracarboxylate Ligand: Syntheses, Structures and Photoluminescent Properties. *Dalton Trans.* **2015**, *44*, 5746–5754.

(12) Wang, C.; Li, L.; Bell, J. G.; Lv, X.; Tang, S.; Zhao, X.; Thomas, K. M. Hysteretic Gas and Vapor Sorption in Flexible Interpenetrated Lanthanide-Based Metal-Organic Frameworks with Coordinated Molecular Gating via Reversible Single-Crystal-to-Single-Crystal Transformation for Enhanced Selectivity. *Chem. Mater.* **2015**, *27*, 1502–1516.

(13) Wu, Y. P.; Li, D. S.; Xia, W.; Guo, S. S.; Dong, W. W. Three Novel Lanthanide Metal-Organic Frameworks (Ln-MOFs) Constructed by Unsymmetrical Aromatic Dicarboxylatic Tectonics: Synthesis, Crystal Structures and Luminescent Properties. *Molecules* **2014**, *19*, 14352–14365.

(14) Das, S. K.; Chatterjee, S.; Bhunia, S.; Mondal, A.; Mitra, P.; Kumari, V.; Pradhan, A.; Bhaumik, A. A New Strongly Paramagnetic Cerium-Containing Microporous MOF for CO 2 Fixation under Ambient Conditions. *Dalton Trans.* **2017**, *46*, 13783–13792.

(15) Liu, Y. H.; Chien, P. H. A Series of Lanthanide-Organic Frameworks Possessing Arrays of 2D Intersecting Channels within a 3D Pillar-Supported Packed Double-Decker Network and Co2+-Induced Luminescence Modulation. *CrystEngComm* **2014**, *16*, 8852–8862.

(16) Nandi, G.; Thakuria, R.; Titi, H. M.; Patra, R.; Goldberg, I. Synthesis, Structure, Topology and Magnetic Properties of New Coordination Polymers Based on 5(-Br/-COOH)-Substituted Nicotinic Acid. *CrystEngComm* **2014**, *16*, 5244–5256.

(17) Nandi, G.; Titi, H. M.; Thakuria, R.; Goldberg, I. Solvent Dependent Formation of Metallogels and Single-Crystal MOFs by La(III) and Ce(III) Connectors and 3,5-Pyridinedicarboxylate. *Cryst. Growth Des.* **2014**, *14*, 2714–2719.

(18) Silva, P.; Ananias, D.; Bruno, S. M.; Valente, A. A.; Carlos, L. D.; Rocha, J.; Almeida Paz, F. A. Photoluminescent Metal-Organic Frameworks - Rapid Preparation, Catalytic Activity, and Framework Relationships. *Eur. J. Inorg. Chem.* **2013**, *2013*, 5576–5591.

(19) Jia, L. N.; Hou, L.; Wei, L.; Jing, X. J.; Liu, B.; Wang, Y. Y.; Shi, Q. Z. Five Sra Topological Ln(III)-MOFs Based on Novel Metal-Carboxylate/Cl Chain: Structure, near-Infrared Luminescence and Magnetic Properties. *Cryst. Growth Des.* **2013**, *13*, 1570–1576.

(20) Tang, Q.; Liu, S.; Liu, Y.; Miao, J.; Li, S.; Zhang, L.; Shi, Z.; Zheng, Z. Cation Sensing by a Luminescent Metal-Organic Framework with Multiple Lewis Basic Sites. *Inorg. Chem.* **2013**, *52*, 2799–2801.

(21) Nayak, S.; Nayek, H. P.; Pietzonka, C.; Novitchi, G.; Dehnen, S. A Series of Three-Dimensional Lanthanide MOFs: Observation of Reversible Structural Changes Controlled by Solvent Desorption-Adsorption, and Magnetic Properties. *J. Mol. Struct.* **2011**, *1004*, 82–87.

(22) Han, Y.; Li, X.; Li, L.; Ma, C.; Shen, Z.; Song, Y.; You, X. Structures and Properties of Porous Coordination Polymers Based on Lanthanide Carboxylate Building Units. *Inorg. Chem.* **2010**, *49*, 10781–10787.

(23) Neofotistou, E.; Malliakas, C. D.; Trikalitis, P. N. Remarkable Structural Diversity and Single-Crystal-to-Single-Crystal Transformations in Sulfone Functionalized Lanthanide MOFs. *CrystEngComm* **2010**, *12*, 1034–1037.

(24) Devic, T.; Wagner, V.; Guillou, N.; Vimont, A.; Haouas, M.; Pascolini, M.; Serre, C.; Marrot, J.; Daturi, M.; Taulelle, F.; et al. Synthesis and Characterization of a Series of Porous Lanthanide Tricarboxylates.

Microporous Mesoporous Mater. **2011**, *140*, 25–33.

(25) Pan, L.; Adams, K. M.; Hernandez, H. E.; Wang, X.; Zheng, C.; Hattori, Y.; Kaneko, K. Porous Lanthanide-Organic Frameworks: Synthesis, Characterization, and Unprecedented Gas Adsorption Properties. *J. Am. Chem. Soc.* **2003**, *125*, 3062–3067.

(26) Lamberti, C.; Zecchina, A.; Groppo, E.; Bordiga, S. Probing the Surfaces of Heterogeneous Catalysts by in Situ IR Spectroscopy. *Chem. Soc. Rev.* **2010**, *39*, 4951.

(27) Bordiga, S.; Scarano, D.; Spoto, G.; Zecchina, A.; Lamberti, C.; Otero Areán, C. Infrared Study of Carbon Monoxide Adsorption at 77 K on Faujasites and ZSM-5 Zeolites. *Vib. Spectrosc.* **1993**, *5*, 69–74.

(28) Vindigni, F.; Manzoli, M.; Tabakova, T.; Idakiev, V.; Boccuzzi, F.; Chiorino, A. Effect of Ceria Structural Properties on the Catalytic Activity of Au–CeO2 Catalysts for WGS Reaction. *Phys. Chem. Chem. Phys.* **2013**, *15*, 13400.

(29) Smolders, S.; Lomachenko, K. A.; Bueken, B.; Struyf, A.; Bugaev, A. L.; Atzori, C.; Stock, N.; Lamberti, C.; Roeffaers, M. B. J.; De Vos, D. Unravelling the Redox-Catalytic Behavior of Ce4+-MOFs: A XAS Study. *ChemPhysChem* **2017**, *19*, 373–378.

(30) Myers, A. L.; Prausnitz, J. M. Thermodynamics of Mixed-gas Adsorption. *AIChE J.* **1965**, *11*, 121–127.

(31) Simon, C. M.; Smit, B.; Haranczyk, M. PyIAST: Ideal Adsorbed Solution Theory (IAST) Python Package. *Comput. Phys. Commun.* **2016**, *200*, 364–380.